JACS
JOURNAL OF THE AMERICAN CHEMICAL SOCIETY

ARTICLE

pubs.acs.org/JACS

Polymer Brushes on Graphene

Marin Steenackers,[†,‡,#] Alexander M. Gigler,[§] Ning Zhang,[‡] Frank Deubel,[‡] Max Seifert,[†] Lucas H. Hess,[†] Candy Haley Yi Xuan Lim,[⊥] Kian Ping Loh,[⊥] Jose A. Garrido,[†] Rainer Jordan,[‡,∥] Martin Stutzmann,[†] and Ian D. Sharp*[,†]

[†]Walter Schottky Institut and Physik Department, Technische Universität München, Am Coulombwall 4, 85748 Garching, Germany

[‡]Wacker-Lehrstuhl für Makromolekulare Chemie, Technische Universität München, Lichtenbergstrasse 4, 85747 Garching, Germany

[§]CeNS and Department of Earth and Environmental Sciences, Ludwig-Maximilians-Universität München, Theresienstrasse 41, 80333 Munich, Germany

[⊥]Department of Chemistry, National University of Singapore, 3 Science Drive 3, Singapore 117543

[∥]Professur für Makromolekulare Chemie, Department Chemie, Technische Universität Dresden, Zellescher Weg 19, 01069 Dresden, Germany

Supporting Information

ABSTRACT: A critical bottleneck for the widespread use of single layer graphene is the absence of a facile method of chemical modification which does not diminish the outstanding properties of the two-dimensional sp^2 network. Here, we report on the direct chemical modification of graphene by photopolymerization with styrene. We demonstrate that photopolymerization occurs at existing defect sites and that there is no detectable disruption of the basal plane conjugation of graphene. This method thus offers a route to define graphene functionality without degrading its electronic properties. Furthermore, we show that photopolymerization with styrene results in self-organized intercalative growth and delamination of few layer graphene. Under these reaction conditions, we find that a range of other vinyl monomers exhibits no reactivity with graphene. However, we demonstrate an alternative route by which the surface reactivity can be precisely tuned, and these monomers can be locally grafted via electron-beam-induced carbon deposition on the graphene surface.

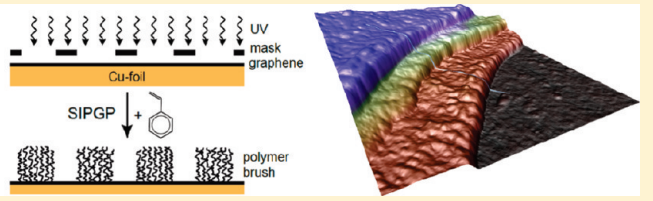

INTRODUCTION

Graphene is an ideal two-dimensional material with exceptional structural, chemical, and electrical properties which make it an extremely promising candidate for biosensing and bioelectronic applications. Recently, the utility of this material has been demonstrated for detecting single molecules,[1−3] sensing pH changes and protein adsorption,[4−6] and monitoring cell action potentials.[7] Furthermore, we have demonstrated that graphene solution gated field effect transistors (SGFETs) have the potential to far exceed even the most advanced Si-based devices in terms of noise and sensitivity.[8] However, in order to realize the full potential of graphene for such applications, methods of achieving defined and specific chemical functionality on material produced using scalable methods must be developed. In this respect, graphene functionalization represents a new challenge compared to other solid-state materials, since covalent molecular binding can lead to significant defect generation which adversely affects electrical transport in the material. Therefore, a careful balance between functionality and carrier mobility must be achieved using precisely controllable chemical methods.

Although a variety of recent reports have demonstrated both noncovalent and covalent molecular modification of graphene,[9−28] the range of existing covalent, yet nondestructive, functionalization strategies remains limited. Noncovalent routes to graphene functionalization, which typically include $\pi-\pi$ stacking using aromatic molecular groups[9−13,29] or ionic interactions between end-functional molecules and edge-functional graphene,[14,15] have the advantage that the structural and electrical quality of the material can be maintained. While such systems have significant potential for a range of applications, covalent chemical functionalization is desirable for devices which must be exposed to harsh environments for long times, such as biological and chemical sensors. Furthermore, noncovalent strategies can limit the range of subsequent chemical processes which can be applied to the physisorbed molecules. Nevertheless, noncovalent bulk polymer−graphene composites are extremely promising for a wide range of mechanical, thermal, and electrical applications.[30−32]

Ideally, approaches to covalent functionalization of graphene would provide the desired chemical activity without adversely affecting electrical transport. Perhaps the most common method of molecular grafting to graphene is based on diazonium chemistry.[16−20] However, under typical reaction conditions, attachment occurs at both edge and basal plane sites, leading to generation

Received: February 2, 2011
Published: June 03, 2011

of sp^3 defects and significant reduction of electrical conductivity.[16,19,20] Similarly, other methods of covalent functionalization of graphene are effective but are expected to disrupt basal plane conjugation.[21−23] Nevertheless, it was recently reported that selective spontaneous reaction of diazonium salts at edge sites is possible in the absence of surfactant[18] and that organosilane-based functionalization occurs selectively at existing oxygen defects.[24,25]

Polymer brushes offer the possibility of providing multiple selective functional sites on each grafted polymer chain while allowing for the design of biosensors with large loading capacities and high sensitivities.[33] Furthermore, covalently bound polymer chains provide both stable and soft environments which are compatible with direct immobilization of biomolecules.[34] Surface-initiated polymerization (SIP) from chemically defined self-assembled monolayers (SAMs) on solid surfaces has been extensively utilized for the formation of polymer brush layers with well controlled functionality, thickness, and density with near-molecular precision.[35] Similar strategies were also employed on both graphene oxide and graphene to grow polymer brushes by means of SIP. Until now, reactive graphene oxide was used to couple suitable initiators for surface-initiated atom transfer radical polymerization (ATRP) of different vinyl monomers.[36−38] Alternatively, the spontaneous grafting of diazonium salts onto graphene[16] was used to attach ATRP-initiators.[39,40] However, the use of SAMs leads to some practical limitations. In particular, the low thermal and chemical stabilities of commonly used SAM systems can complicate subsequent polymerization and side group modification reactions. Furthermore, activation of the graphene can disturb the basal plane conjugation via sp^2 to sp^3 bond conversion.[16,19,21−23]

Recently, direct photografting reactions of vinyl monomers came into focus for the preparation of stable polymer brushes. Two approaches in particular, the sequential "living" photopolymerization[41] and the self-initiated photografting and photopolymerization (SIPGP),[42−44] attracted the attention of numerous research groups because of the facile preparation and broad applicability. While in the first, benzophenone is photochemically grafted onto a native substrate to form a photoinitiator for the successive photografting, the SIPGP is a facile one-step process that uses the monomer itself as the photosensitizer. Both processes rely on a radical abstraction mechanism from the surface, and first comparative studies by Frechet et al.[45] showed that no significant differences can be observed between the two approaches. Especially if the SIPGP is performed in bulk monomer, AFM studies indicate the formation of dense polymer brush layers of preferably linear chains.[46] Recently, we have shown that well-defined, homogeneous, and highly stable polymer brushes can be prepared directly on carbonaceous materials, such as diamond,[47] glassy carbon,[48] carbon-polar hexagonal SiC,[49] and electron-beam-induced carbon deposits[50] by the SIPGP process with vinyl monomers. The formation of defined reactive interlayers, such as SAMs, is no longer necessary, and polymer brushes can be prepared in a single-step reaction. Furthermore, the SIPGP approach allows the preparation of micro- and nanostructured polymer brushes on various noncarbonaceous substrates by means of the carbon templating (CT) technique.[50] The excellent chemical and thermal stabilities of the polymer brush layers allow consecutive polymer analogue reactions, even under drastic conditions.[47] By this approach, stable polymer brushes with different shapes, dimensions, polymer architectures, and chemical functionalities can be prepared on a variety of substrates.[42,48−50]

Here, we show that the UV-induced polymerization of styrene yields homogeneous polystyrene (PS) brush layers directly and covalently bound to graphene. Since the only requirement for successful SIPGP is the availability of abstractable hydrogen atoms on the surface for radical initiation of the reaction under UV illumination,[47,49,50] pristine graphene is expected to exhibit no reactivity with the vinyl monomers investigated here. However, we explore the possibility of using edge and basal plane defects to allow an analogous photopolymerization process without disturbing the conjugation of the as-prepared material. This process is applied to graphene produced via each of the most scalable, technologically promising methods: CVD graphene on Cu, epitaxial graphene on SiC, and reduced graphene oxide. Raman spectroscopy reveals that the grafting reaction results in no detectable disruption to the conjugation of the graphene, indicating that binding sites are primarily limited to existing defects. Hall effect measurements further confirm that the high carrier mobilities of graphene are not significantly affected by photopolymerization. Surprisingly, comparison of polymer thickness and morphology following growth on single and few layer graphene samples provides evidence for intercalative growth and delamination of few layer graphene (FLG). In addition, we find that a range of other investigated vinyl monomers exhibits no reactivity with the graphene surface under the present reaction conditions. However, we show that the nonreactive monomers can be utilized for formation of structured polymer brush layers via local electron-beam-induced carbon deposition (EBCD) on the graphene surface.

EXPERIMENTAL SECTION

Graphene Growth and Preparation. CVD graphene films were fabricated in a thermal CVD furnace using copper foil as the substrate, similar to methods reported previously.[51,52] All reactions were carried out with the graphene on the Cu foil. After the photopolymerization of styrene (vide infra), the functionalized CVD graphene was thoroughly rinsed with toluene, ethyl acetate, and ethanol in order to remove physisorbed polymer. The Cu foil was then etched overnight using aqueous 1 M $(NH_4)_2S_2O_8$ solution. After the total dissolution of the Cu foil, the functionalized graphene sheet remained floating on the $(NH_4)_2S_2O_8$ solution and could clearly be observed with the naked eye. The functionalized graphene sheet was then rinsed with distilled water and transferred onto 300 nm SiO_2 on Si.

Epitaxial graphene on SiC was formed using the high-temperature sublimation method. The SiC samples were diced into 10×5 mm^2 crystals. After degreasing with ethanol, the samples were introduced into an annealing station housed in an ultrahigh vacuum (UHV) chamber equipped with reflection high-energy electron diffraction (RHEED). The SiC substrates were dosed with silicon from an evaporation source for 3 min to enrich the surface with silicon. This was followed by a series of annealing steps (1 min) between 900 to 1300 °C. Flash annealing was performed until a $(6\sqrt{3} \times 6\sqrt{3})$-R30° reconstruction pattern appeared as monitored by RHEED. The sample was removed from the UHV chamber and transferred in air to a scanning tunneling microscopy (STM) chamber for further annealing and analysis. The presence of a long-range Moiré pattern characteristic of honeycomb graphene confirmed that the epitaxial graphene had been successfully prepared on the surface, and the sample was removed for further processing. The thicknesses of the graphene layers were characterized using peak profile analysis and substrate feature attenuation in Raman spectroscopy.[53,54] In order to study the effect of graphene coverage on photopolymerization, different samples with a single layer and up to 10 layers of graphene were utilized. Atomic force micrographs of typical single and few layer

graphene on SiC samples are provided in the Supporting Information (Figure S1).

Reduced graphene oxide (RGO) was prepared in two stages. Graphene oxide (GO) was first prepared using a modified Hummers method from graphite powders (grade 230 U kindly provided by Asbury Graphite Mills, Inc.). Hydrazine-reduced GO was subsequently obtained by adding 10 mL of 98% hydrazine solution into 10 mL of 0.5 mg/mL GO solution. The reduction process was carried out at 50 °C for 12 h. The RGO flakes were collected by filtration, washed with pure water several times, and dried at 90 °C.

Surface Photopolymerization. Polymerization was performed by immersing graphene in ~2 mL of freshly distilled and degassed bulk monomer and irradiation with UV fluorescent lamp with a spectral distribution between 300 and 400 nm (intensity maximum at $\lambda = 350$ nm with a total power of ~5 mW/cm^2). Polymerization and grafting reactions were performed with a range of vinyl monomers, including styrene, methyl methacrylate (MMA), *N*,*N*-dimethylaminoethyl methacrylate (MAEMA), methacrylatoethyl trimethyl ammonium chloride (METAC), and 4-vinyl pyridine (4VP) on CVD graphene, epitaxial graphene on SiC, and reduced graphene oxide. After UV irradiation, the samples were removed from the bulk monomer and thoroughly rinsed with a series of several solvents (e.g., toluene, ethyl acetate, and ethanol for the case of styrene) to ensure that only chemically grafted polymer remained on the substrate.

Patterned photopolymerization was achieved on CVD graphene on Cu by UV illumination through a photomask. The samples were clamped with a 400 mesh Cu TEM grid (hole width: 58 μm, bar width: 25 μm; Plano GmbH). Photopolymerization, cleaning, and transfer were then performed as described above.

We note that all photopolymerization reactions on CVD-grown graphene on Cu and epitaxial graphene on SiC were performed under identical conditions at the Technische Universität München. Although photopolymerization on RGO was performed at the National University of Singapore under similar conditions, the reaction rates of the two systems cannot be directly compared.

Electron Beam-Induced Carbon Deposition. A 10×50 μm^2 carbon template gradient was prepared by direct writing with a focused electron beam on graphene using a Zeiss E-line scanning electron microscope. The electron beam energy was set at 3 keV with a current of 136 pA and a vacuum pressure of $\sim 5 \times 10^{-6}$ mbar. The electron dose was continuously increased from 0 to 20 mC/cm^2. Atomic force microscopy (AFM) of the EBCD gradient revealed that the deposited carbon had a maximum thickness of approximately 0.5 nm, as shown in Figure S2 of the Supporting Information. Following EBCD, polymerization was performed using the methods described above.

Atomic Force Microscopy (AFM). AFM scans were performed with a multimode scanning probe microscope from Veeco Instruments using standard tips in tapping mode under ambient conditions. The measurement of the covalently grafted, unstructured polymer brush thickness on the epitaxial single and few layer graphene on 6H-SiC was performed by scratching the polymer layer with a metallic needle. The border of the scratch was then imaged by AFM in tapping mode over an area of 10 μm^2. The scanned data were analyzed by the local depth analysis option of the commercial AFM software by choosing areas within the scratched region and the intact surface around the trench.

Fourier Transform Infrared Spectroscopy. Infrared spectroscopy was performed following polymerization of CVD-grown graphene with an IFS Bruker instrument equipped with a diffuse reflectance infrared Fourier transform (DRIFT) setup from SpectraTech and a liquid nitrogen-cooled MCT detector. For each spectrum, 470 scans were accumulated with a spectral resolution of 4 cm^{-1}. The measurements were performed on functionalized CVD graphene transferred onto 300 nm SiO_2 on Si. For each measurement, background spectra were recorded on bare 300 nm SiO_2 on Si.

Hall Effect Measurements. Hall effect measurements were performed on CVD graphene transferred to 300 nm SiO_2 on Si. Pressed indium contacts were formed in the van der Pauw geometry on $\sim 1 \times 1$ cm^2 graphene samples. Measurements were performed using a Keithley 6220 precision current source, a Keithley 181 Nanovoltmeter, and a 0.345 T permanent magnet.

Raman Spectroscopy. Confocal Raman microscopy (alpha 300R, WITec GmbH, Ulm, Germany) was used to evaluate the effect of polymerization on the graphene. Following patterned photopolymerization of styrene monomer, the CVD grown graphene on Cu was transferred to 300 nm SiO_2 on Si, as described above. Raman mapping was performed over a 59×54 μm^2 region, which included both UV illuminated and masked regions, with a step size of 220 nm and an integration time of 0.4 s. The excitation wavelength was 532 nm using a 2ω-Nd:YAG solid-state laser. In order to prevent damage to the graphene or PS, the laser power was limited to 5 mW. We used a standard 100× microscope objective with a high numerical aperture (NA = 0.9) in order to efficiently collect the scattered light from the sample. For the case of graphene on SiC, background subtraction was required to remove substrate-related features.

RESULTS AND DISCUSSION

Surface-Initiated Polymerization by Photografting and Photopolymerization (SIPGP). Direct photografting of styrene was performed on single layer graphene grown via chemical vapor deposition on Cu foil, as outlined in Figure 1. Under nitrogen, the substrate was immersed in freshly distilled bulk styrene and irradiated for approximately 16 h with UV light with a spectral distribution between 300 and 400 nm (intensity maximum at $\lambda = 350$ nm with a total power of ~5 mW/cm^2). After the photopolymerization, the substrate was rigorously rinsed with different organic solvents in order to remove physisorbed polymer. The Cu foil was then etched in ammonium persulfate solution, and the resulting free-standing functionalized graphene sheet was transferred onto a 300 nm thick SiO_2 film on Si. Commonly, graphene must be mechanically stabilized during the transfer process by either a spin-on photoresist or a heat release tape.[51,52] Here, such a layer was not necessary because the grafted PS layer sufficiently stabilized the graphene and allowed for photoresist-free transfer onto arbitrary substrates. Such a stabilizing effect, which facilitates handling, was also observed for the preparation of so-called polymer carpets, polymer brush layers grown by SIPGP on 1 nm thin highly cross-linked monolayers.[55,56]

The presence of grafted polystyrene chains on the transferred graphene sheet was confirmed by DRIFT spectroscopy. As shown in Figure 2a, the characteristic vibrational modes of PS are observed, including the aromatic groups (ν_{C-H} at ~3024 cm^{-1} and ν_{C-C} between 1454 and 1601 cm^{-1}) and the methylene groups of the polymer backbone (ν_{C-H} ~2919 cm^{-1}).[57]

In order to assess the effect of photopolymerization on the graphene, elucidate the bonding mechanism, and to further investigate covalent attachment, scanning confocal Raman scattering measurements were performed following local polymerization. Patterned polymer brush layers were prepared on graphene grown by CVD on Cu according to the methods presented in Figure 1. The single layer graphene on Cu sample was placed in the styrene monomer and illuminated with UV light through a shadow mask, resulting in selective reaction in the illuminated regions. Due to the large luminescence background from the underlying foil, it was not possible to obtain high-quality Raman spectra from Cu-supported graphene. Therefore, the measurements

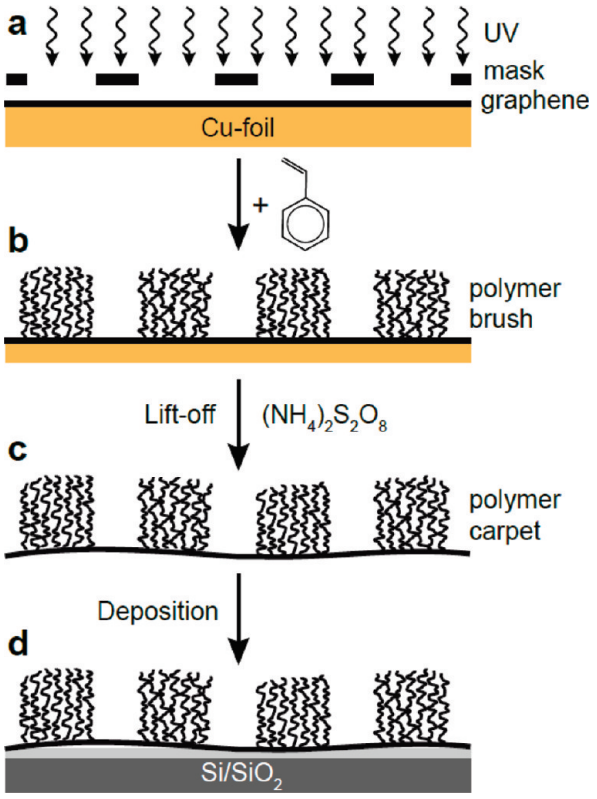

Figure 1. Patterned polymer brush layers on CVD-grown single layer graphene are prepared by UV illumination through a mask in bulk styrene. Surface photopolymerization occurs selectively in illuminated regions of the material. Photoresist-free transfer of the polymer carpet on graphene onto 300 nm SiO_2 on Si is achieved using standard etching techniques.

were performed on transferred material. Also for the case of patterned polymer, no spin-on photoresist or heat release tape was necessary for the transfer.

The effect of spectral overlap must be considered when analyzing Raman scattering data from the two-component PS-graphene system. Figure 2b shows a comparison of the Raman spectra from graphene and bulk PS. While the observed modes are well separated in the region near the 2D graphene band, there is significant spectral overlap in the region of the D and G bands. Therefore, for quantitative analysis of the D and G mode intensities, the appropriate PS contribution to the total scattering intensity was subtracted from each region of interest based on reference data and the PS intensity at the maximum near 3055 cm^{-1}. Figure 2c shows the portion of the Raman spectrum near the 2D mode obtained in an illuminated region which contains contributions from both PS and graphene. Though the total contribution from PS is small, the signal is readily resolved.

Raman mapping of patterned samples allowed direct and simultaneous measurement of the effect of polymerization on the structure of graphene (i.e., defect generation via sp^2 to sp^3 bond conversion)[58] as well as possible strain[59] and doping[60] effects. Figure 2d shows the integrated PS scattering intensity in the range of 3000−3100 cm^{-1} following a 16 h reaction. Importantly, PS is observed only in the UV illuminated region, indicating that all noncovalently bound polymer is removed during the cleaning steps. The corners of the Raman map shown in Figure 2d, in which there is no PS, can be used for direct comparison to areas which have undergone reaction. Figure 2e shows the integrated D/G mode intensity ratio in the same region. The observed structure is attributed to the grain edges which are characterized by large defect densities.[61] Despite the observation of local edge state-related inhomogeneities, there is no correlation between the defect-related scattering intensity and the presence or absence of PS. Figure 2f shows a comparative histogram of the D/G intensity ratios in polymerized and nonpolymerized regions from a sample reacted for 16 h. No change of the D/G intensity ratio is observed. In addition, within the photopolymerized region, no direct spatial correlation between the defect-induced scattering intensity and the PS scattering intensity is observed. While local regions of higher defect concentration are detected, it is important to note that a defect-related peak is present at all locations within the measured region. This suggests that basal plane defects are viable sites for initiation. However, these results indicate that, under the present reaction conditions, the UV-initiated photopolymerization reaction does not generate a large amount of basal plane defects and that photografting occurs preferentially at existing defect sites.

Hall effect measurements were performed before and after photopolymerization and confirmed that the electronic properties of graphene are not adversely affected by the PS grafting reaction. Following transfer to SiO_2, the graphene exhibited p-type conduction with a mobility of 580 $cm^2/(V\,s)$ at a hole concentration of 7×10^{12} cm^{-2}. High levels of hole doping are well-known for graphene transferred to SiO_2 and have been attributed to interfacial and atmospheric water.[62,63] Following reaction, the hole concentration was reduced to 2×10^{12} cm^{-2}, and the mobility increased to 800 $cm^2/(V\,s)$, most likely due to reduced interactions with water in the presence of hydrophobic PS. An important consequence of this selective reactivity is that the photografting process results in covalently grafted PS brushes that provide a versatile chemical handle for tailored functionality,[47] while simultaneously maintaining the outstanding electronic properties of the underlying graphene.

At present, the specific mechanism of photopolymerization initiation is not clear. However, for the case of the SIPGP reaction mechanism, abstractable hydrogen must be present on the substrate surface. It has recently been demonstrated that silanization reactions, which selectively occur at hydroxyl surface sites, can be applied to both highly ordered pyrolytic graphite (HOPG) and single layer graphene.[24] Such hydroxyl moieties are expected to be suitable for initiation of SIPGP.

Intercalative Polymer Brush Growth. In order to demonstrate the broad applicability of direct photografting on graphene, the reaction was also performed on epitaxially grown single and few layer graphene on SiC as well as on RGO. In both cases, dense PS brush layers were formed, as in the case of CVD graphene.

Investigation of the SiC-graphene-polymer brush composites by AFM reveals continuous and uniform layers. To determine the thickness of the PS layer, the surface was scratched with a metallic needle in order to locally remove the organic PS layer(s). The borders of the scratches were investigated by AFM to measure the height difference and thus the brush layer thickness (Figure 3a−c).[49] Detailed analysis of the scanned data on different analog scratches showed that a homogeneous 16 ± 4 nm thick PS brush layer was formed on single layer graphene (Figure 3a). Remarkably, simultaneous polymerization on few layer graphene samples yielded homogeneous layer thicknesses of 160 ± 8 and 270 ± 10 nm for 6 and 10 layer graphene, respectively (Figure 3b

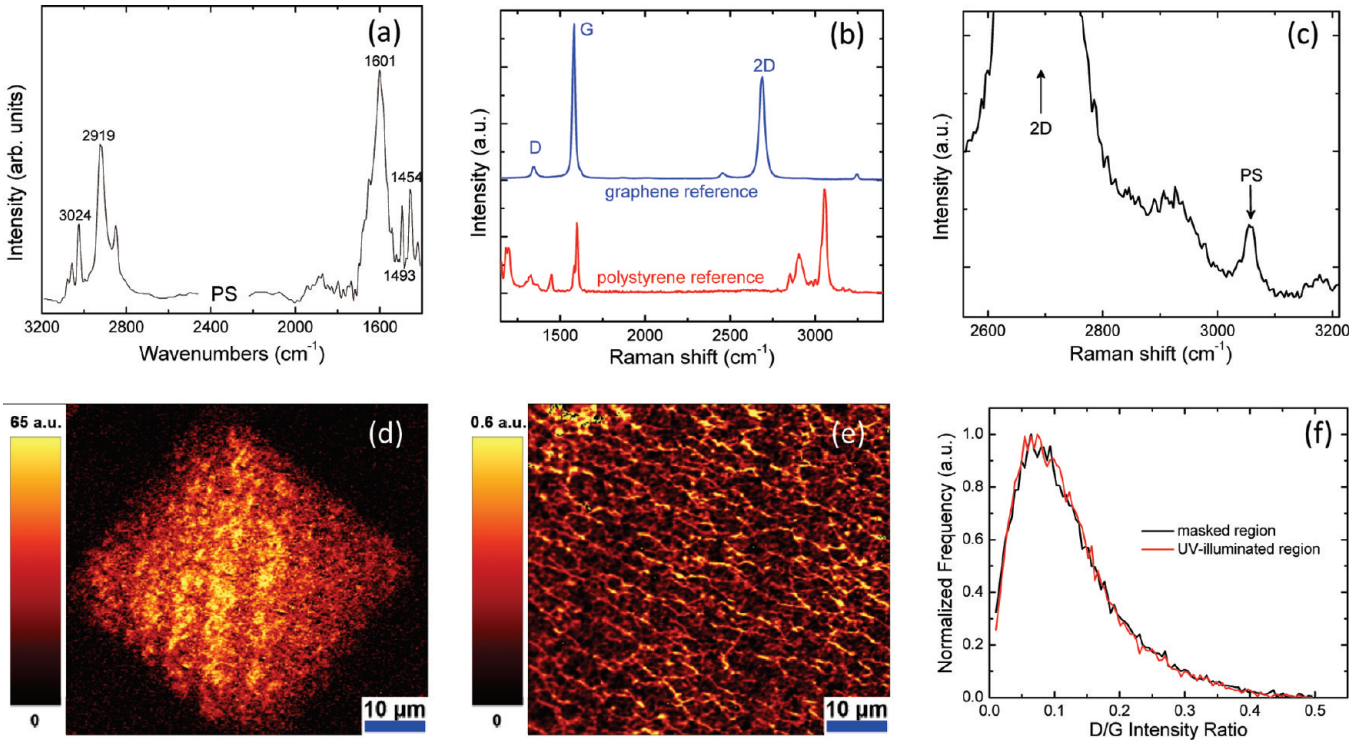

Figure 2. (a) Infrared absorption spectrum of a functionalized single layer CVD graphene on Cu after transfer onto a 300 nm thick SiO_2 film on Si. Monomer: styrene; photopolymerization time: 16 h; polymer thickness: 10 nm. (b) Comparative Raman spectra from as-grown graphene transferred to 300 nm SiO_2 on Si and bulk polystyrene. (c) Raman spectrum obtained following photopolymerization which shows the primary PS peak with an intensity ~40× smaller than the graphene 2D mode. (d) Raman map of the integrated intensity from PS in the range of 3000−3100 cm^{-1} following patterned photopolymerization by selective UV illumination through a shadow mask. (e) The D/G intensity ratio over the same region. (f) Normalized histograms of the D/G mode intensity ratio in regions with PS (UV illuminated) and without PS (masked). No detectable increase of the defect-activated D mode intensity is observed following photopolymerization.

and c). As shown in Figure 3d, the polymer−graphene composite thickness increases with the number of graphene layers with a slope of approximately 28 nm/layer. Since SIPGP on single layer graphene yields a polymer brush thickness of ~16 nm, it is possible to conclude that polymerization on monolayer graphene occurs on a single side only, whereas intercalation of styrene between additional graphene layers leads to simultaneous reaction on two sides, as shown in the inset of Figure 3d. Thus, the total thickness is expected to scale approximately as $2n - 1$, where n is the number of graphene layers. However, absorption of incident UV light by graphene is expected to result in deviations from this ideal behavior and in a reduction of the reaction rate for underlying layers. As shown in Figure 3b, this general behavior is observed. Nevertheless, for the FLG thicknesses investigated here, this effect does not lead to significant deviations, within the measurement error, from a linear thickness increase with the number of graphene layers. In agreement with the findings from CVD graphene, Raman spectra obtained before and after photopolymerization indicate no increase of the D to G mode intensity ratio following reaction, as shown in Figure S3 of the Supporting Information. This result confirms that polymerization initiation is limited to existing defect sites and does not significantly affect the conjugated graphene network.

Further analysis of AFM data obtained at the borders of the scratched regions of FLG/PS shows the presence of multilayered structures with step heights of several tens of nanometers (Figure 3b and c). Similar layer morphologies, with varying numbers of steps, were observed for several independent polymerization experiments on different epitaxially grown FLG samples. The measured step heights are also plotted in Figure 3d and correspond well with the fitted line obtained from the total thickness measurements.

Finally, photopolymerization of styrene was performed on flakes of FLG obtained from reduced graphene oxide samples. As shown by the AFM analysis in Figure 3e after the polymerization in styrene, the resulting RGO/PS composite exhibited a stepped structure with nearly equal step heights between successive layers, similar to the FLG/PS described above. However, we note that the reaction conditions for RGO were not identical to those for the other samples, and quantitative comparison of layer thicknesses is not possible in this case. Nevertheless, results obtained on multiple samples, including two types of FLG prepared using very different methods, are in full qualitative agreement and consistently indicate that such a morphology is characteristic of interlayer PS brush formation for FLG.

We have previously reported surface polymerization on a wide range of other substrates, none of which exhibited the stepped morphology described here.[42,47−50] Together, the scaling of the polymer layer thickness with number of graphene layers (Figure 3d) and the stepped morphology of FLG flakes as well as at scratch edges strongly suggest a delamination of the graphene sheets of FLG and formation of polymer brushes between the layers by styrene monomer intercalation during the grafting reaction (Figure 3d inset). This conclusion is also supported by the good agreement between the step heights and the total thickness as a function of the number of graphene layers.

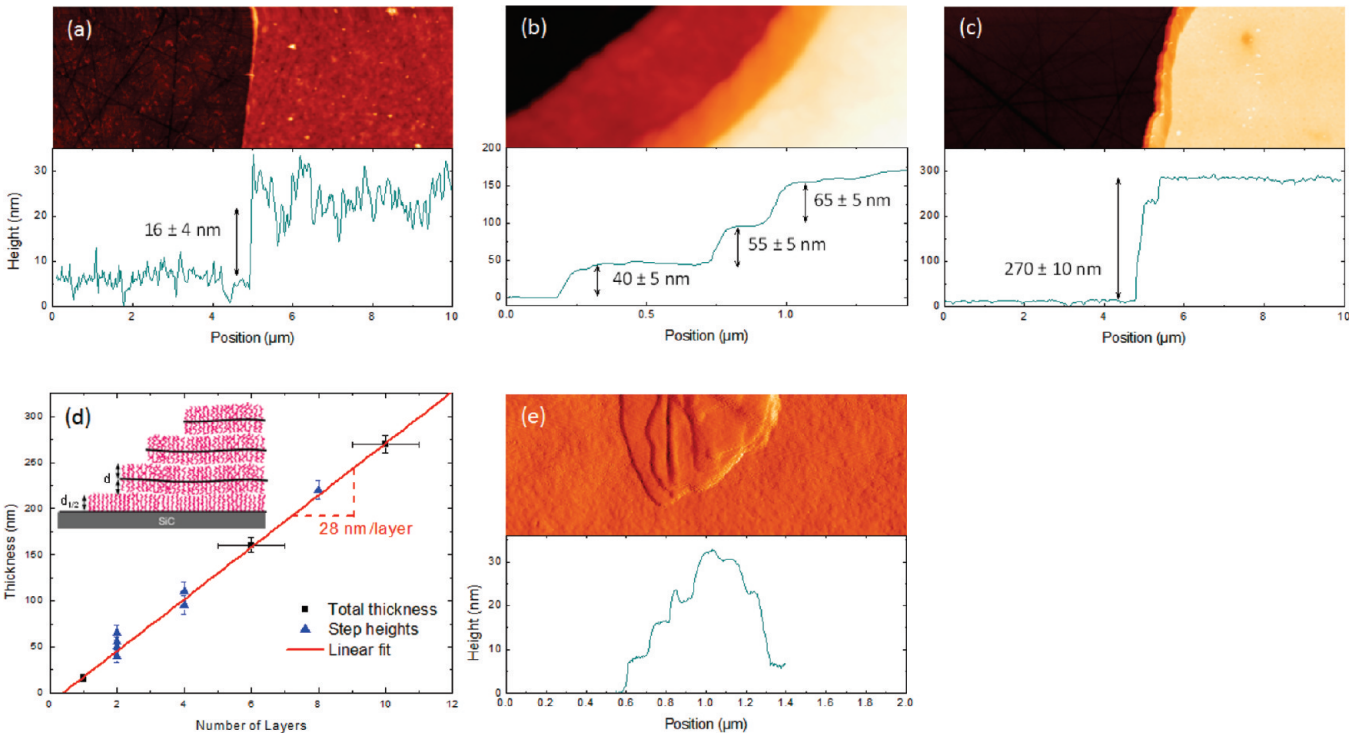

Figure 3. AFM and height profiles at scratch edges following styrene photopolymerization (16 h) on graphene. The material was grown epitaxially on SiC and consists of: (a) a single layer, (b) 6 layer, and (c) 10 layer graphene. Few layer graphene samples (b and c) exhibit a step-like morphology at the scratch edge. (d) Plot of the polymer carpet thickness as a function of number of graphene layers on SiC for 16 h of reaction with styrene (■). Also shown are the measured step heights (▲) at the scratch edge. The inset of (d) shows a schematic illustration of the intercalative growth of polystyrene brushes between layers of few layer graphene. (e) Atomic force amplitude image and corresponding height profile from a flake of few layer reduced graphene oxide following photopolymerization. As in the case of FLG on SiC (b and c), RGO exhibits a stepped structure which highlights the intercalative growth process characteristic of SIPGP on FLG.

To the best of our knowledge, between-layer polymerization of styrene has only been reported for preprocessed graphite intercalation compounds (GICs).[65−67] However, it was recently reported that direct solvent exfoliation of graphite is possible when the surface tension of the solvent matches well that of graphene.[68,69] In such cases, the solvent−graphene interaction compensates the energy required for exfoliation. Reported values for the room temperature surface tension of PS are in the range of 35−40 mJ/m^2, with values increasing with the average polymer molar mass.[70] This range of values is lower than, but nevertheless close to, the ideal value for exfoliation of graphite (∼40−50 mJ/m^2).[68] We note that a range of surface energies for graphene has been reported and may depend strongly on the presence of defects. It is, thus, conceivable that the balance of surface energies leads to an intercalative polymerization. Alternatively, it has been suggested that charge transfer through $\pi-\pi$ stacking between molecules, such as pyridine and graphite layers, may contribute to exfoliation.[71] Presently, the specific mechanism of the intercalative growth of PS on FLG under UV activation is not known, and a detailed investigation of this intriguing behavior will be the subject of future research.

Selective Reactivity of Vinyl Monomers. Photopolymerization on both CVD grown graphene on Cu and few layer epitaxial graphene on SiC was also attempted with a range of other vinyl monomers including methyl methacrylate (MMA), *N*,*N*-dimethylaminoethyl methacrylate (MAEMA), methacrylatoethyl trimethyl ammonium chloride (METAC), and 4-vinyl pyridine (4VP) under the given reaction conditions. We found that of all the tested monomers, only styrene resulted in polymer brush layers on graphene, as measured on both patterned and unpatterned CVD material and by scratching measurements on epitaxial samples.

Our results clearly indicate that the grafting process of styrene on graphene is photoactivated and occurs primarily at existing defect sites with no or only minimal conversion of sp^2 to sp^3 carbon in the graphene lattice. One possible grafting mechanism is via a self-initiated photografting and photopolymerization mechanism in which the monomer itself acts as the photosensitizer.[43,44] Although we and others have shown that SIPGP can be employed with a wide variety of vinyl monomers and multiple substrates,[42,48−50,72] a selective self-initiation of styrene and a few other monomers on some substrates has also been reported[64] and points to a specific monomer−substrate interaction during photoactivation.

Carbon Templating for Structured Polymer Brush Growth. Recently, we reported on the preparation of micro- and nanostructured polymer brushes on various inorganic substrates by means of carbon templating (CT).[48,49] This initiator-, photoresist-, and mask-free process is similar to the dip-pen lithography technique developed by Mirkin et al.[73] However, instead of a SAM, a stable carbon template layer is locally written by EBCD and then structurally amplified by the selective formation of polymer brush layers of controlled three-dimensional shapes by means of SIPGP, as shown schematically in Figure 4a. The formation of polymer brushes on EBCD-treated surfaces by the SIPGP mechanism can be explained by the low bond

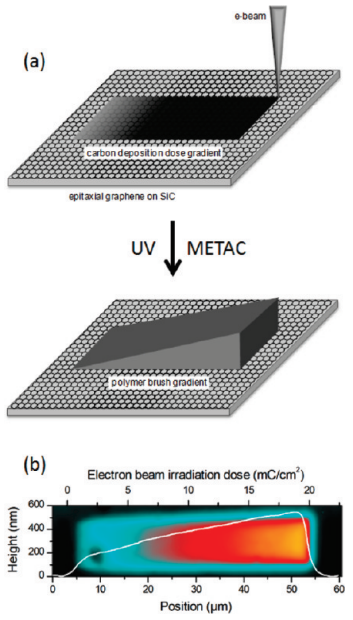

Figure 4. (a) Schematic of the carbon templating process for the formation of structured polymer brushes with controlled thicknesses. Photopolymerization is performed following patterned electron beam-induced carbon deposition. (b) Height profile of a ($10 \times 50\ \mu m^2$) poly(METAC) brush layer formed on an electron beam-deposited carbon gradient on few layer graphene on SiC. The electron dose was linearly increased from 0 to 20 mC/cm^2. The polymer grafting density, and hence the thickness, increases with increasing electron dose. The background image shows the two-dimensional AFM image of the selected region.

dissociation energy (BDE) for hydrogen abstraction from the carbon deposits.[50] Since this approach requires a reactivity contrast between the bare substrate and the carbon deposits, structured PS brushes on graphene cannot be prepared by CT. However, since all other tested vinyl monomers exhibited no reactivity toward graphene, this technique is well-suited for providing structured polymer brushes from functional vinyl monomers on graphene. In this work, a $10 \times 50\ \mu m^2$ carbon template gradient was prepared on FLG on SiC by direct e-beam writing with a continuous electron dose increase from 0 to 20 mC/cm^2. The substrate was subsequently immersed in an aqueous METAC solution and irradiated with UV for 1 h. Following reaction, the sample was subjected to rigorous cleaning with different solvents in ultrasound in order to ensure that only covalently bound polymer chains remained on the surface. As shown in Figure 4b, AFM measurements reveal the formation of a poly(METAC) brush layer selectively grown on the carbon template region with a thickness which is predetermined by the locally applied electron dose. The increase of the polymer layer thickness with electron dose is in agreement with earlier work.[50] At low doses, the carbon deposits only partially cover the substrate, and the polymer layer thickness is proportional to the surface concentration of potential grafting points.[50] The continuous increase of the poly(METAC) brush thickness on the patterned graphene surface can be explained by an increase of the polymer grafting density. We note that the polymerization rate for METAC is significantly faster than for PS on graphene, which is due to the faster rate of radical reactions of methacrylates compared to styrene. This observation is also consistent with previous observations of monomer-dependent reaction rates on other surfaces.[44,49,50,74] This result demonstrates that structured polymer brushes can be formed on graphene using the CT technique with monomers which exhibit no reactivity to pristine graphene. Since the polymer brush thickness can be tuned by controlling the locally applied electron dose, the formation of well-defined and complex three-dimensional structures from macroscopic down to nanometer scales is possible.[50]

CONCLUSION

In conclusion, covalently bound polystyrene brush layers can be formed on graphene by direct photografting and photopolymerization. The broad applicability of this technique was demonstrated via growth on CVD graphene, epitaxial single and few layer graphene on SiC, and reduced graphene oxide. Scanning Raman spectroscopy on patterned polymer brush layers indicated that photopolymerization does not cause any detectable disruption of the basal plane conjugation of graphene. Furthermore, electrical transport measurements indicate that the exceptional electronic properties of graphene are retained following photopolymerization. From these results, we conclude that initiation of the polymerization reaction occurs at existing defect sites.

Atomic force microscopy on photopolymerized few layer graphene indicated an enhanced polymerization rate with increasing number of layers and a stepped morphology at scratch edges and on reduced graphene oxide flakes. The specific mechanism for the delamination of graphene sheets and intercalated growth, which appears to be characteristic of styrene photopolymerization on few layer graphene, may be due to a balance of surface forces or an as yet unidentified charge-transfer process. Additional work is underway to determine the processes responsible for this behavior. Nevertheless, such self-organized structures could find great use for bottom-up assembly of devices, including ultracapacitors and graphene-based biosensors.

Unexpectedly, vinyl monomers other than styrene were found to be not reactive with graphene under the present conditions. However, this reactivity contrast provides a means of achieving patterned polymer brush structures on graphene using electron beam-induced carbon deposition. These findings provide a route to truly multifunctional polymer brushes and polyelectrolytes on graphene surfaces, e.g., via copolymerization or subsequent polymer analog reactions with PS brushes.[50] Together, these results provide a powerful new set of tools for nanoscale covalent chemical functionalization of graphene.

ASSOCIATED CONTENT

Supporting Information. AFM of single and few layer graphene on SiC prior to polymerization, AFM of the as-deposited carbon template on graphene, Raman spectra from multilayer graphene on SiC before and after photopolymerization, and full author list for ref 68. This material is available free of charge via the Internet at http://pubs.acs.org.

AUTHOR INFORMATION

Corresponding Author
*sharp@wsi.tum.de.

Present Address
[#]Chemical Physics of Materials (Catalysis-Tribology), Universite Libre de Bruxelles (U.L.B.) - Faculte des Sciences, Departement de Chemie, Campus Plaine CP 243, B-1050 Bruxelles, Belgium

■ ACKNOWLEDGMENT

This work was supported by the Technische Universität München—Institute for Advanced Study, the Nanosystems Initiative Munich (NIM), and the International Graduate School of Science and Engineering (IGSSE), all funded by the German Excellence Initiative, as well as the German Research Foundation (DFG) in the framework of the Priority Program 1459 "Graphene". K.P.L. thanks the NRF-CRP grant "Graphene and Related Materials and Devices" R-143-000-360-281. We are also grateful to Robert W. Stark for allowing the use of facilities in his laboratory at LMU-München for Raman measurements.

■ REFERENCES

(1) Schedin, F.; Geim, A. K.; Morozov, S. V.; Hill, E. W.; Blake, P.; Katsnelson, M. I.; Novoselov, K. S. *Nat. Mater.* **2007**, *6*, 652–655.
(2) Dan, Y.; Lu, Y.; Kybert, N. J.; Luo, Z.; Johnson, A. T. C. *Nano Lett.* **2009**, *9*, 1472–1475.
(3) Garaj, S.; Hubbard, W.; Reina, A.; Kong, J.; Branton, D.; Golovchenko, J. A. *Nature* **2010**, *467*, 190–193.
(4) Ohno, Y.; Maehashi, K.; Yamashiro, Y.; Matsumoto, K. *Nano Lett.* **2009**, *9*, 3318–3322.
(5) Ang, P. K.; Chen, W.; Wee, A. T. S.; Loh, K. P. *J. Am. Chem. Soc.* **2008**, *130*, 14392–14393.
(6) Cheng, Z.; Li, Q.; Li, Z.; Zhou, Q.; Fang, Y. *Nano Lett.* **2010**, *10*, 1864–1868.
(7) Cohen-Karni, T.; Qing, Q.; Li, Q.; Fang, Y.; Lieber, C. M. *Nano Lett.* **2010**, *10*, 1098–1102.
(8) Dankerl, M.; Hauf, M. V.; Lippert, A.; Hess, L. H.; Birner, S.; Sharp, I. D.; Mahmood, A.; Mallet, P.; Veuillen, J.-Y.; Stutzmann, M.; Garrido, J. A. *Adv. Funct. Mater.* **2010**, *20*, 3117–3124.
(9) Su, Q.; Pang, S.; Alijani, V.; Li, C.; Feng, X.; Müllen, K. *Adv. Mater.* **2009**, *21*, 3191–3195.
(10) Xu, Y.; Bai, H.; Lu, G.; Li, C.; Shi, G. *J. Am. Chem. Soc.* **2008**, *130*, 5856–5857.
(11) Wang, Y.; Chen, X.; Zhong, Y.; Zhu, F.; Loh, K. P. *Appl. Phys. Lett.* **2009**, *95*, 063302.
(12) Liu, J.; Tao, L.; Yang, W.; Li, D.; Boyer, C.; Wuhrer, R.; Braet, F.; Davis, T. P. *Langmuir* **2010**, *26*, 10068–10075.
(13) Zhang, J.; Lei, J.; Pan, R.; Xue, Y.; Ju, H. *Biosens. Bioelectron.* **2010**, *26*, 371–376.
(14) Liang, Y.; Wu, D.; Feng, X.; Müllen, K. *Adv. Mater.* **2009**, *21*, 1679–1683.
(15) Choi, E.-Y.; Han, T. H.; Hong, J.; Kim, J. E.; Lee, S. H.; Kim, H. W.; Kim, S. O. *J. Mater. Chem.* **2010**, *20*, 1907.
(16) Bekyarova, E.; Itkis, M. E.; Ramesh, P.; Berger, C.; Sprinkle, M.; de Heer, W. A.; Haddon, R. C. *J. Am. Chem. Soc.* **2009**, *131*, 1336–1337.
(17) Zhu, Y.; Higginbotham, A. L.; Tour, J. M. *Chem. Mater.* **2009**, *21*, 5284–5291.
(18) Lim, H.; Lee, J. S.; Shin, H.-J.; Shin, H. S.; Choi, H. C. *Langmuir* **2010**, *26*, 12278–12284.
(19) Sharma, R.; Baik, J. H.; Perera, C. J.; Strano, M. S. *Nano Lett.* **2010**, *10*, 398–405.
(20) Hossain, M. Z.; Walsh, M. A.; Hersam, M. C. *J. Am. Chem. Soc.* **2010**, *132*, 15399–15403.
(21) Liu, H.; Ryu, S.; Chen, Z.; Steigerwald, M. L.; Nuckolls, C.; Brus, L. E. *J. Am. Chem. Soc.* **2009**, *131*, 17099–17101.
(22) Liu, L.-H.; Lerner, M. M.; Yan, M. *Nano Lett.* **2010**, *10*, 3754–3756.
(23) Quintana, M.; Spyrou, K.; Grzelczak, M.; Browne, W. R.; Rudolf, P.; Prato, M. *ACS Nano* **2010**, *4*, 3527–3533.
(24) Lee, B.; Chen, Y.; Duerr, F.; Mastrogiovanni, D.; Garfunkel, E.; Andrei, E. Y.; Podzorov, V. *Nano Lett.* **2010**, *10*, 2427–2432.
(25) Yang, H.; Li, F.; Shan, C.; Han, D.; Zhang, Q.; Niu, L.; Ivaska, A. *J. Mater. Chem.* **2009**, *19*, 4632.
(26) Wang, Q. H.; Hersam, M. C. *Nat. Chem.* **2009**, *1*, 206–211.
(27) Pramoda, K. P.; Hussain, H.; Koh, H. M.; Tan, H. R.; He, C. B. *J. Polym. Sci., A: Polym. Chem.* **2010**, *48*, 4262–4267.
(28) Sun, S.; Cao, Y.; Feng, J.; Wu, P. *J. Mater. Chem.* **2010**, *20*, 5605.
(29) Wang, Q. H.; Hersam, M. C. *Nat. Chem.* **2009**, *1*, 206–211.
(30) Vickery, J. L.; Patil, A. J.; Mann, S. *Adv. Mater.* **2009**, *21*, 2180–2184.
(31) Bocking, T.; Abdala, A. A.; Stankovich, S.; Dikin, D. A.; Herrera-Alonso, M.; Piner, R. D.; Adamson, D. H.; Schniepp, H. C.; Chen, X.; Ruoff, R. S.; Nguyen, S. T.; Aksay, I. A.; Prud'Homme, R. K.; Brinson, L. C. *Nat. Nanotechnol.* **2008**, *3*, 327–331.
(32) Stankovich, S.; Dikin, D. A.; Dommett, G. H. B.; Kohlhaas, K. M.; Zimney, E. J.; Stach, E. A.; Piner, R. D.; Nguyen, S. T.; Ruoff, R. S. *Nature* **2006**, *442*, 282–286.
(33) Harsányi, G. *Mater. Chem. Phys.* **1996**, *43*, 199–203.
(34) Padeste, C.; Farquet, P.; Potzner, C.; Solak, H. H. *J. Biomater. Sci. Polym. Ed.* **2006**, *17*, 1285–1300.
(35) Jordan, R., Ed. Surface-Initiated Polymerization I & II (in Advances in Polymer Science vol. 197 & 198), Springer, 2006.
(36) Yang, Y.; Wang, J.; Zhang, J.; Liu, J.; Yang, X.; Zhao, H. *Langmuir* **2009**, *25*, 11808–11814.
(37) Gonçalves, G.; Marques, P. A. A. P.; Barros-Timmons, A.; Bdkin, I.; Singh, M. K.; Emami, N.; Grácio, J. *J. Mater. Chem.* **2010**, *20*, 9927.
(38) Lee, S. H.; Dreyer, D. R.; An, J.; Velamakanni, A.; Piner, R. D.; Park, S.; Zhu, Y.; Kim, S. O.; Bielawski, C. W.; Ruoff, R. S. *Macromol. Rapid Commun.* **2010**, *31*, 281–288.
(39) Fang, M.; Wang, K.; Lu, H.; Yang, Y.; Nutt, S. *J. Mater. Chem.* **2010**, *20*, 1982.
(40) Fang, M.; Wang, K.; Lu, H.; Yang, Y.; Nutt, S. *J. Mater. Chem.* **2009**, *19*, 7098.
(41) Ma, H.; Davis, R. H.; Bowman, C. N. *Macromolecules* **2000**, *33*, 331–335.
(42) Steenackers, M.; Küller, A.; Stoycheva, S.; Grunze, M.; Jordan, R. *Langmuir* **2009**, *25*, 2225–2231.
(43) Deng, J.-P.; Yang, W.-T.; Rånby, B. *Macromol. Rapid Commun.* **2001**, *22*, 535–538.
(44) Wang, H.; Brown, H. R. *Macromol. Rapid Commun.* **2004**, *25*, 1095–1099.
(45) Stachowiak, T. B.; Svec, F.; Fréchet, J. M. J. *Chem. Mater.* **2006**, *18*, 5950–5957.
(46) Wang, H.; Brown, H. R. *Polymer* **2007**, *48*, 477–487.
(47) Steenackers, M.; Lud, S. Q.; Niedermeier, M.; Bruno, P.; Gruen, D. M.; Feulner, P.; Stutzmann, M.; Garrido, J. A.; Jordan, R. *J. Am. Chem. Soc.* **2007**, *129*, 15655–15661.
(48) Zhang, N.; Steenackers, M.; Luxenhofer, R.; Jordan, R. *Macromolecules* **2009**, *42*, 5345–5351.
(49) Steenackers, M.; Sharp, I. D.; Larsson, K.; Hutter, N. A.; Stutzmann, M.; Jordan, R. *Chem. Mater.* **2010**, *22*, 272–278.
(50) Steenackers, M.; Jordan, R.; Küller, A.; Grunze, M. *Adv. Mater.* **2009**, *21*, 2921–2925.
(51) Bae, S.; Kim, H.; Lee, Y.; Xu, X.; Park, J.-S.; Zheng, Y.; Balakrishnan, J.; Lei, T.; Ri Kim, H.; Song, Y. I.; Kim, Y.-J.; Kim, K. S.; Ozyilmaz, B.; Ahn, J.-H.; Hong, B. H.; Iijima, S. *Nat. Nanotechnol.* **2010**, *5*, 574–578.
(52) Li, X.; Cai, W.; An, J.; Kim, S.; Nah, J.; Yang, D.; Piner, R.; Velamakanni, A.; Jung, I.; Tutuc, E.; Banerjee, S. K.; Colombo, L.; Ruoff, R. S. *Science* **2009**, *324*, 1312–1314.
(53) Shivaraman, S.; Chandrashekhar, M.; Boeckl, J.; Spencer, M. *J. Elect. Mat.* **2009**, *38*, 725–730.
(54) Ferrari, A. C.; Meyer, J. C.; Scardaci, V.; Casiraghi, C.; Lazzeri, M.; Mauri, F.; Piscanec, S.; Jiang, D.; Novoselov, K. S.; Roth, S.; Geim, A. K. *Phys. Rev. Lett.* **2006**, *97*, 187401.

(55) Amin, I.; Steenackers, M.; Zhang, N.; Beyer, A.; Zhang, X.; Pirzer, T.; Hugel, T.; Jordan, R.; Gölzhäuser, A. *Small* **2010**, *6*, 1623–1630.
(56) Amin, I.; Steenackers, M.; Zhang, N.; Schubel, N.; Beyer, A.; Gölzhäuser, A.; Jordan, R. *Small* **2011**, *7*, 683–687.
(57) Hesse, M. M. *Spektroskopische Methoden in der Organischen Chemie*; Georg Thieme Verlag: Stuttgart, Germany, 1995.
(58) Graf, D.; Molitor, F.; Ensslin, K.; Stampfer, C.; Jungen, A.; Hierold, C.; Wirtz, L. *Nano Lett.* **2007**, *7*, 238–242.
(59) Mohiuddin, T. M. G.; Lombardo, A.; Nair, R. R.; Bonetti, A.; Savini, G.; Jalil, R.; Bonini, N.; Basko, D. M.; Galiotis, C.; Marzari, N.; Novoselov, K. S.; Geim, A. K.; Ferrari, A. C. *Phys. Rev. B* **2009**, *79*, 205433.
(60) Das, A.; Pisana, S.; Chakraborty, B.; Piscanec, S.; Saha, S. K.; Waghmare, U. V.; Novoselov, K. S.; Krishnamurthy, H. R.; Geim, A. K.; Ferrari, A. C.; Sood, A. K. *Nat. Nanotechnol.* **2008**, *3*, 210–215.
(61) Li, X.; Cai, W.; Colombo, L.; Ruoff, R. S. *Nano Lett.* **2009**, *9*, 4268–4272.
(62) Novoselov, K. S.; Geim, A. K.; Morozov, S. V.; Jiang, D.; Zhang, Y.; Dubonos, S. V.; Grigorieva, I. V.; Firsov, A. A. *Science* **2004**, *306*, 666–669.
(63) Cao, H.; Yu, Q.; Jauregui, L. A.; Tian, J.; Wu, W.; Liu, Z.; Jalilian, R.; Benjamin, D. K.; Jiang, Z.; Bao, J.; Pei, S. S.; Chen, Y. P. *Appl. Phys. Lett.* **2010**, *96*, 122106.
(64) Deng, J.; Wang, L.; Liu, L.; Yang, W. *Prog. Polym. Sci.* **2009**, *34*, 156–193.
(65) Shioyama, H. *Carbon* **1997**, *35*, 1664–1665.
(66) Chen, G.; Wu, D.; Weng, W.; He, B.; Yan, W. *Polym. Int.* **2001**, *50*, 980–985.
(67) Xiao, M.; Sun, L.; Liu, J.; Li, Y.; Gong, K. *Polymer* **2002**, *43*, 2245–2248.
(68) Hernandez, Y.; et al. *Nat. Nanotechnol.* **2008**, *3*, 563–568.
(69) Liang, Y. T.; Hersam, M. C. *J. Am. Chem. Soc.* **2010**, *132*, 17661–17663.
(70) Chee, K. K. *J. Appl. Polym. Sci.* **1998**, *70*, 697–703.
(71) Bourlinos, A. B.; Georgakilas, V.; Zboril, R.; Steriotis, T. A.; Stubos, A. K. *Small* **2009**, *5*, 1841–1845.
(72) Hutter, N. A.; Reitinger, A.; Zhang, N.; Steenackers, M.; Williams, O. A.; Garrido, J. A.; Jordan, R. *Phys. Chem. Chem. Phys.* **2010**, *12*, 4360.
(73) Piner, R. D.; Zhu, J.; Hong, S.; Mirkin, C. A. *Science* **1999**, *283*, 661–663.
(74) Steenackers, M.; Küller, A.; Stoycheva, S.; Grunze, M.; Jordan, R. *Langmuir* **2009**, *25*, 2225–2231.